Anisotropic viscous effects of local flow by a rotating microparticle in nematic liquid crystal

Jun-Yong Lee,[1] Jae Hoon Lee,[1] Bohdan Lev,[2] and Jong-Hyun Kim[1,3,*]

[1]*Department of Physics, Chungnam National University, 99 Daehak-ro, Yuseong-gu, Daejeon, 34134, Korea*

[2]*Bogolyubov Institute for Theoretical Physics of the NAS of Ukraine, Metrolohichna Str.14-b, Kyiv, 03680, Ukraine*

[3]*Institute of Quantum Systems, Chungnam National University, Daejeon, 34134, Korea*

(Received 10 October 2021; revised 16 May 2022; accepted 29 June 2022; published 25 July 2022)

The presented study opens a perspective to investigate the effects of local flow on nematic liquid crystals. A particle rotated in nematic fluids typically generates a rotationally symmetric local flow, which causes a change in the director orientation. The director above the threshold velocity has a particular angle determined by the ratio of Leslie coefficients, α_2/α_3. In 5CB liquid crystals, this director angle with respect to the flow is approximately 13°. The angle is calculated through Ericksen-Leslie theory. The angle is not dependent on rotation frequency or particle size but temperature. The area of the influenced region increases with the rotation frequency and particle size. The changes in radius of the influenced region are calculated theoretically using Ericksen number. Further, an interference pattern appears at the edge of the influenced region by the refractive indexes mismatch between the influenced region and the rest. We experimentally obtain the thickness of the influenced region analyzing intervals of the pattern.

DOI: 10.1103/PhysRevE.106.014706

I. INTRODUCTION

Nematic liquid crystals (NLCs) have not only fluidity but also long-range orientational ordering between molecules, which distinguishes them from isotropic fluids. The most remarkable features of NLCs are an appropriate degree of elasticity and various anisotropies on the macroscopic scale [1,2]. Liquid crystal (LC) molecules tend to align in an orientation similar to that of adjacent molecules, where the average orientation is called the director. The director can be controlled by external fields, the properties of the substrates in which the LCs are constrained, and so on [3]. Furthermore, flow is also one of the most important factors that influence the director; in particular, the direction and gradient of the flow play a critical role. We can observe not only changes in the alignment of the director but also various instabilities of the system by generating a flow in a uniformly aligned LC cell [4–9]. Rich responses of the LC director can result from different types of shear flow and shapes of the cell confining the LCs [10–15].

In nematic fluid research, the anisotropy of viscosity in addition to flow is also important. Anisotropy of viscosity can be expressed through Miesowicz viscosity and Leslie coefficients, and the hydrodynamics of nematic fluids can be analyzed through the theories from Ericksen and Leslie [16–20]. From anisotropic viscosity, we can observe many interesting phenomena that do not appear in isotropic fluids [21–26]. For example, a Poiseuille flow in a uniformly and obliquely aligned LC to the flow creates transverse pressure [27]. Additionally, because the sign and magnitude of the coefficients play an important role in determining the size or orientation of the phenomena, many studies on various physical quantities of LCs have been conducted [28–32].

To date, most research on the behavior of LCs has focused on large-scale flow, while the effects of local flow on LCs have received relatively less attention. Among the studies on the effects of local flow, Rovner *et al.* observed various phenomena resulting from dispersed ferromagnetic discs rotated by a magnetic field in uniformly aligned LCs [33]. They pointed out that the alignment of the director around each disc changes when the angular velocity of the disc exceeds a certain threshold, and also that the relaxation of the phenomena is affected by the ratio between elasticity and viscosity when rotation is stopped [33]. However, they did not investigate the alignment change of the director further or the cause of the change in detail. In the present work, we experimentally generate a local flow on the single-particle scale using micro-sized ferromagnetic spheres in NLCs and a rotating magnetic field. We apply Ericksen-Leslie theory on this scale and reveal not only the details of the director alignment in the region where the flow exceeds the threshold velocity and its cause but also the shape of the region where the alignment change happens. The related phenomena are calculated through the viscous torque exerted on the director and the proposed model that considers the distance from the substrate in the Ericksen number.

II. EXPERIMENTS

We used a mixture of NLCs and spherical ferromagnetic particles in a rotating magnetic field to generate a local flow. The mixture was prepared through the following process. Ferromagnetic spheres approximately 8–30 μm in diameter were dispersed into deionized water at a concentration of 1%. The ferromagnetic spherical particles (CFM-80-5 and CFM-

*Corresponding author: jxk97@cnu.ac.kr

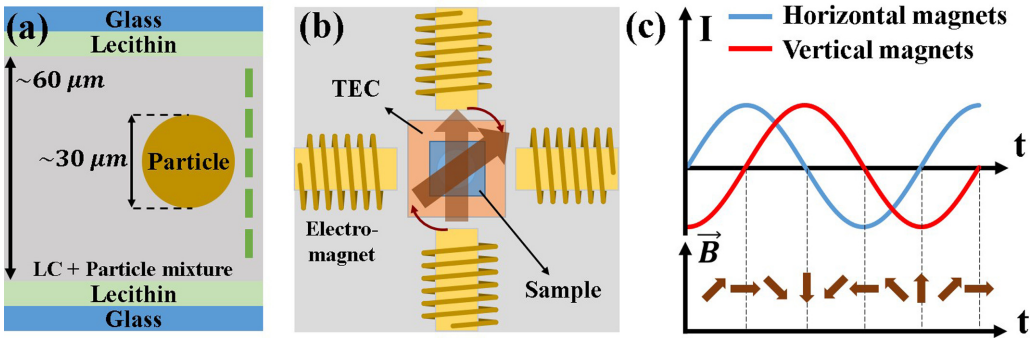

FIG. 1. (a) Schematic diagram of the sample structure. (b) Schematic diagram of the stage in which an in-plane rotating magnetic field can be applied to samples. TEC represents a thermoelectric cooler. (c) Plot of the direction of the magnetic field as a function of time.

300-5, Spherotech) comprise a polystyrene core and a CrO_2 thin outer layer; the mass ratio of CrO_2 is about 3–5%. The polystyrene and CrO_2 were approximately 1.05 g/cm^3 and 4.89 g/cm^3 in density, respectively, so that the particles were slightly denser than the NLCs at 1.01 g/cm^3. Next, we put the deionized water and particle mixture into vials and dried in a fume hood for 1 to 2 days. We then added 4-Cyano-4′-pentylbiphenyl (5CB) or N-(4-Methoxybenzylidene)-4-butylaniline (MBBA) into the vials. The 5CB and particle mixture was used in all the experiments except for when observing the temperature dependency of the results.

We conducted experiments with cells in which the director was vertically aligned to the substrates. The cells were made by sandwiching two sheets of glass coated with lecithin with a cell gap of 60 μm using double-sided tape. Before coating the glass with lecithin, it was cleaned with detergent, acetone, and ethanol using a sonicator for 15 min, after which it was dried at about 70 °C for 15 min. The mixtures were then injected into the prepared cells [Fig. 1(a)].

The samples were placed on a stage in which an in-plane rotating magnetic field was applied using four electromagnets [Fig. 1(b) and 1(c)]. Each electromagnet was arranged at 90° with respect to the adjacent magnets and had a phase difference of $\pi/2$. The magnetic field was approximately 50 gauss in amplitude and 0.1–2 Hz in frequency. We limited the range of frequency to 2 Hz in this experiment as the textures around the rotating particles drastically changed over roughly 2 Hz, differing by particle. We controlled the temperature using a thermoelectric cooler. We observed the behavior of the particles in response to varying magnetic field rotation frequency and temperature through a polarizing optical microscope.

III. RESULTS AND DISCUSSION

We observed the phenomena appearing around rotating particles with a rotation axis parallel to the director in a homeotropic cell. We interpreted the phenomena through the viscous anisotropy and the Ericksen number that compares the flow and the elastic properties.

A. Director alignment around a rotating particle

The rotating particles created a surrounding distinct region under crossed polarizers, implying that a change in the director alignment appeared around the particles. We also observed a dark cross around the particles [Figs. 2(a) and 2(b)]. This dark cross was oppositely oblique against the rotating direction of the particles. When we rotated a polarizer and an analyzer counterclockwise at the same time, the dark cross also rotated at the same degree [Fig. 2(d)]. This means that the alignment of the director around the rotating particles has rotational symmetry and also that the orientation of the director in the dark cross coincides with the orientation of the polarizer or the analyzer. We also obtained images by rotating only the polarizer with no analyzer [Fig. 2(e)]. In this case, only light with a polarization parallel to the polarizer reaches the sample. Because scattering by thermal fluctuation of the director is stronger when the polarization is parallel to the director than when it is not, such a region looks darker [34]. Considering the overall information from Fig. 2, we determine that the director is aligned with an orientation close to the tangent of the particles. We can obtain theoretical values of the orientation of the director from the calculation described in the following paragraphs. The director around a counterclockwise rotating particle is aligned parallel with the polarizer at $\psi = 77°$ or with an analyzer at $\psi = -13°$ [Fig. 2(c)], where ψ is defined in Fig. 2(a).

A rotating particle produces a flow that has the same velocity as that of the particle surface. The flow spreads to the bulk and tends to change the director alignment. On the other hand, the elasticity of the NLCs resists this alteration. The relation between flow and elasticity is expressed by the Ericksen number. When the velocity of the flow exceeds the threshold value, a transition of the director alignment occurs. The director above the threshold velocity of the flow is aligned at a particular angle with respect to the shear flow, which is called the Leslie angle. We theoretically calculated the angle through Ericksen-Leslie theory [16–20] as below, and compared the calculated director alignment to the experimental data.

Consider the coordinate system in Fig. 3. To express the alignment of the director, a torque exerted on the director is necessary. Viscous torque under certain flow can be written as

$$\boldsymbol{\Gamma} = -\boldsymbol{n} \times (\gamma_1 \boldsymbol{N} + \gamma_2 \boldsymbol{A}\boldsymbol{n}), \tag{1}$$

where $\boldsymbol{N} = D\boldsymbol{n}/Dt - \boldsymbol{\Omega} \times \boldsymbol{n}$ is the relative angular velocity of the director, with D/Dt the material derivative [35] and $\boldsymbol{\Omega}$ the vorticity or rate of rotation which can be written as $(\nabla \times \boldsymbol{v})/2$ where $\boldsymbol{v}$ is the velocity vector of the flow in a nematic fluid and v_i is the i^{th} component of the velocity. In

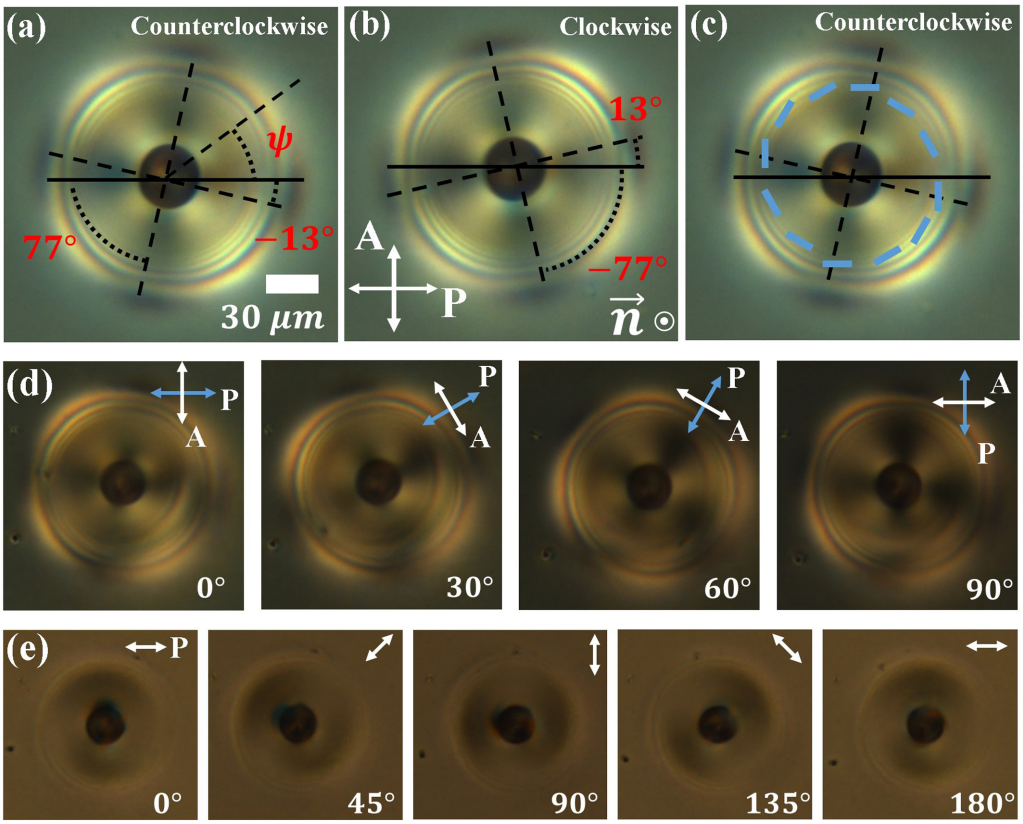

FIG. 2. Images from (a) counterclockwise or (b) clockwise rotating particle under crossed polarizers. An oblique dark cross dependent on the rotation direction appears. (c) Image with a schematic diagram of the director (blue lines) overlaid around the rotating particle. (d) Images from rotating crossed polarizers from 0 to 90°. The director is aligned parallel with the polarizer or analyzer in the dark cross in each image. (e) Images obtained by rotating the polarizer with no analyzer from 0 to 180°. Because scattering is strong at the position where the orientation of the director coincides with the polarization direction of light, the director is aligned parallel with the polarizer in the dark cross. The particle in (d) and (e) rotates counterclockwise.

Eq. (1), $A_{ij} = (\partial v_i/\partial x_j + \partial v_j/\partial x_i)/2$ is the rate of strain, $\boldsymbol{n}$ is the director, $\gamma_1 = \alpha_3 - \alpha_2$ is the rotational viscosity and $\gamma_2 = \alpha_3 + \alpha_2$ is the viscosity that the irrotational flow experiences, and α_i are the Leslie coefficients, which are six coefficients characterizing the anisotropic viscosity connected via Onsager-Parodi relationship. α_2 determines the degree of torque exerted on the director aligned perpendicular to the velocity direction and parallel to the gradient direction, which always has a negative value. α_3 determines the degree of torque on the director aligned parallel to the velocity, which generally has a relatively small value. $\boldsymbol{n}$ can be expressed as $(\sin\theta\cos\phi,\ \sin\theta\sin\phi,\ \cos\theta)$, treating θ as the polar angle and ϕ as the azimuthal angle with the axis perpendicular to the substrate (z axis) [Fig. 3(b)].

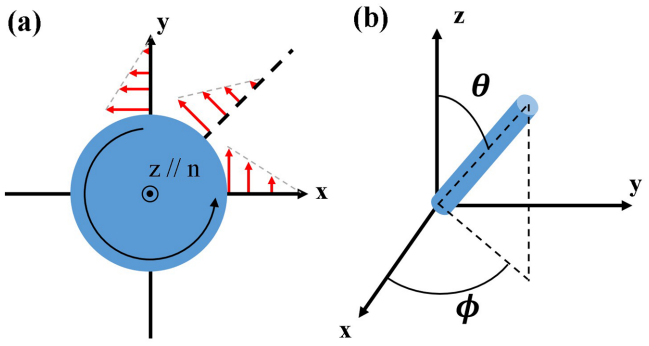

FIG. 3. (a) Schematic diagram of the velocity distribution around a counterclockwise rotating particle. The red arrows indicate velocity vectors. The flow has a tangential velocity that decreases further from the particle. (b) Schematic diagram of the orientation of the director.

We have to know the velocity distribution around a rotating particle to calculate the viscous torque ($\boldsymbol{\Gamma}$). Because a flow has the same velocity as that of the particle surface with a rigid boundary condition and the system has complete rotational symmetry about the rotation axis, velocity occurs in a tangential direction ($\hat{\psi}$) and becomes smaller as it is further away from the particle. $\hat{\psi}$ is a unit vector of the azimuthal angle defined as ψ in Fig. 2(a). Considering that the velocity at the surface is large at the equator and becomes smaller closer to the poles, velocity depends on all (x, y, and z) directions [Fig. 3(a)].

We used two simplifications to explain the observed results in a straightforward manner. First, we focused on calculations on the x axis only. Because the system has complete rotational symmetry, once we calculate the alignment of the director on the x axis, we can easily induce the alignment at different orientations using rotational transformation. For example, if a stable azimuthal angle of the director on the x axis is ϕ_0,

at any angle ψ, the stable azimuthal angle of the director is $\phi_0 + \psi$. Second, we simplified the velocity dependence. We can well explain the phenomena only considering the plane that includes the equator and the vicinity of the plane because their effect on the behavior is dominant. From the spherical geometry of the particles, the velocity at the surface of the particles becomes smaller closer to the poles, so that we can consider that the function of velocity has a form of a sine function about the polar angle. The change in velocity is quite small around $\pi/2$ corresponding to the equator, so that we can neglect velocity dependence in the z direction. Additionally, because v_x is small on the x axis, we can consider velocity in the y direction only. And as v_y is continuous and has even symmetry about the x axis, we can treat $\boldsymbol{v}$ as $\boldsymbol{v_y}(\boldsymbol{x})$. From these simplifications, only A_{xy}, A_{yx}, and Ω_z are valid, and they have the same value of $(1/2)(\partial v_y/\partial x)$. Then, replacing $(1/2)(\partial v_y/\partial x)$ with β, we can obtain the following equations:

$$\boldsymbol{N} = -\boldsymbol{\Omega} \times \boldsymbol{n} = (\beta \sin\theta \sin\phi, -\beta \sin\theta \cos\phi, 0), \tag{2}$$

$$\boldsymbol{An} = (\beta \sin\theta \sin\phi, \beta \sin\theta \cos\phi, 0). \tag{3}$$

From Eqs. (2) and (3), Eq. (1) becomes

$$\boldsymbol{\Gamma} = 2\alpha_2\beta \sin\theta \cos\phi \cos\theta\hat{x} - 2\alpha_3\beta \sin\theta \sin\phi \cos\theta\hat{y} + (2\alpha_3\beta \sin^2\theta\sin^2\phi - 2\alpha_2\beta \sin^2\theta\cos^2\phi)\hat{z} \tag{4}$$

Because the polar angle (θ) is zero at first and all terms include $\sin\theta$, when considering a completely static homeotropic condition, no torque is applied. However, in actuality, there are small n_x, n_y due to thermal fluctuation, so that torque on the x and y directions occurs. The torque on the x and y direction contributes to an increase of n_y and n_x, respectively, resulting in an amplification of the magnitude of n_x and n_y. As a result, θ reaches $\pi/2$, and the x and y components of the torque including $\cos\theta$ disappear, leaving

$$\Gamma_z = 2\beta[\alpha_3\sin^2\phi - \alpha_2\cos^2\phi]. \tag{5}$$

The torque exerted on the director becomes equilibrium at ϕ making Eq. (5) equal zero. Then, we obtain ϕ corresponding to the equilibrium as below,

$$\phi_c = \pm \arctan\left(\sqrt{\frac{\alpha_2}{\alpha_3}}\right). \tag{6}$$

We apply the above equation to the 5CB NLCs, where α_2 and α_3 are approximately -75 mPa s and -4 mPa s, respectively [30]. With these values, ϕ_c is $\pm 77^\circ$. The two angles correspond to unstable and stable equilibrium states. To find out which angle agrees with the stable equilibrium state, we have to advance the analysis of Eq. (5). Considering $\phi = 0, \ -\pi/2$, the viscous torque can be obtained as follows:

$$\Gamma_z\ (at\ \phi = 0) = -2\beta\alpha_2, \tag{7}$$

$$\Gamma_z\left(at\ \phi = -\frac{\pi}{2}\right) = 2\beta\alpha_3. \tag{8}$$

From Fig. 3(a), β in a counterclockwise rotating particle is always negative. Moreover, because both α_2 and α_3 have a negative value, Eq. (7) and Eq. (8) have negative and positive values, respectively. In other words, as the orientation of the director (ϕ) approaches 0 or $-\pi/2$, torque in the counterclockwise or clockwise direction is applied to the director, respectively. Hence, when ϕ_c is -77°, the system is stable for the counterclockwise rotating particle. On the other hand, for the clockwise rotating particle, β has a positive value, so that the system is stable at $\phi_c = 77^\circ$.

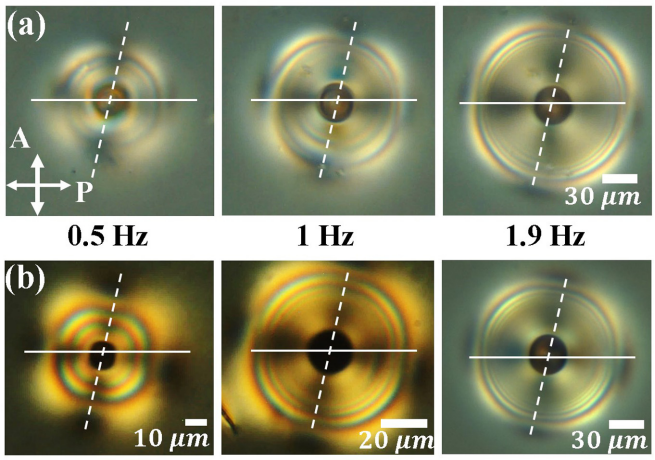

FIG. 4. (a) Images with changing rotation frequencies of a particle with a 30-μm diameter. (b) Images from rotating particles with diameters of 10, 20, and 30 μm. The degree of obliqueness of the dark cross is not dependent on the frequency or diameter of the particle.

Due to the complete rotational symmetry of the system, the orientation of the director at azimuthal angle ψ is $-77^\circ + \psi$ or $77^\circ + \psi$ about a counterclockwise or clockwise rotating particle, respectively. Therefore, the director around a counterclockwise rotating particle is parallel to the analyzer at $\psi = -13^\circ$ or the polarizer at $\psi = 77^\circ$, so that such regions become dark. This calculation agrees with the experimental data [Fig. 2(a)], which indicates that changes in the director alignment under large-scale flow also appear under local flow and that the same means of explanation can be applied in both cases. We note that, for a more detailed explanation, the existence and effects of defects around the particle should be considered. In the present work, because we deal with the region in which the effect of flow overcomes that of elasticity, we excluded the effects of defects around the particle. Nevertheless, the calculation shows a fairly good agreement with the experimental results.

It could be thought that the stable angle, ϕ_c, is dependent on the magnitude of the flow or the size of the particle. However, from Eq. (6), ϕ_c is dependent only on the ratio between α_2 and α_3 and not on other factors. To experimentally prove this, we measured the obliqueness of the dark cross that indicates the stable angle around the rotating particle with varying rotation frequency and particle size. In both cases, the degree of the obliqueness does not change (Fig. 4). This is matched well to the theoretical result.

In fact, the value of the obliqueness of the dark cross in Fig. 2(b) does not exactly agree with the theoretical values. As calculated values can vary depending on the results of particular studies, differences between experimental and theoretical values have been reported [29,30,36]. For example, α_2 and α_3

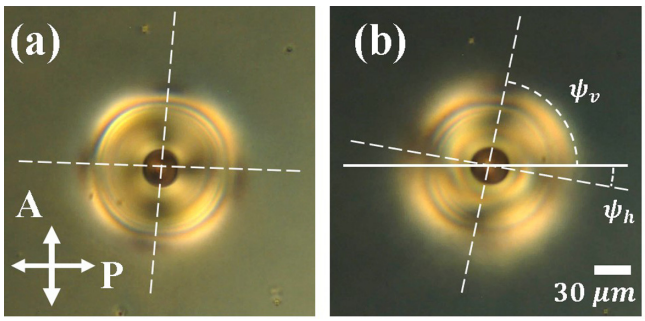

FIG. 5. Images from a counterclockwise rotating particle (a) at room temperature and (b) near the transition temperature. We modified the brightness and contrast to increase clarity.

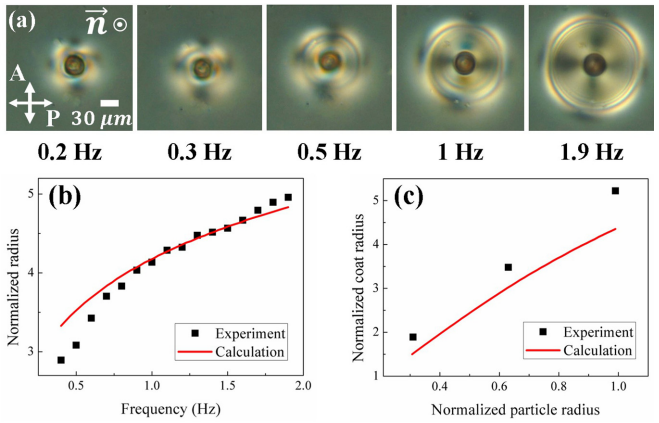

FIG. 6. (a) Textures around a counterclockwise rotating particle with increasing frequency. The region where the alignment changes grows with frequency. (b), (c) Plots of the radius of the region where the alignment changes as a function of frequency and particle radius. We normalized all the length scale with the radius of particle to clarify the characterization of the relative length change. The coat radii in (b) and (c), and particle radius in (c) are normalized by the general particle size we used, 15 μm. The coat radii in (b) and (c) are observed, respectively, with fixed particle size 15 μm and at fixed frequency 2 Hz. The black squares and red line are the experimental and calculated results, respectively.

were found to be, respectively, −75 mPa s and −4 mPa s at 26 °C from Skarp *et al.* with a ϕ_c of about ±77° [37]. Whereas Herba *et al.* reported results of −78 mPa s and −7 mPa s for α_2 and α_3, respectively, with a ϕ_c of approximately ±73.3° [38]. Nonetheless, because many studies support that both values are negative, the stable equilibrium ϕ_c does not change between the two possible ϕ_c angles.

Most physical quantities that determine the properties of LCs are rather sensitive to temperature, and likewise the Leslie coefficients are sensitive as well. Because the range in which 5CB is in the nematic phase is narrow and changes of the Leslie coefficients by temperature are relatively small, it is hard to observe overall behavior changes in images. Hence, we used a mixture of MBBA and particles for observing temperature-dependent variation. From Kneppe *et al.*, α_2 and α_3 are −110 mPa s and -1.1 mPa s at room temperature, and −21 mPa s and -1.8 mPa s at 44 °C [39]. Therefore, ϕ_c in MBBA shows distinguishable differences between room temperature and near the phase transition temperatures; namely, 84° and 74°, respectively. We measured the oblique angles of the dark cross for many particles while controlling temperature (Fig. 5). Defining ψ_h as the angle of the horizontal direction of the dark cross and ψ_v as that of the vertical direction as expressed in Fig. 5(b), we obtained $\psi_h = -3.4° \pm 4.3°$ and $\psi_v = 81.2° \pm 3.2°$ at room temperature and $\psi_h = -8.4° \pm 2.7°$ and $\psi_v = 77.7° \pm 2.8°$ near the transition temperature. These shifts correspond to the tendency of the Leslie coefficients by temperature. However, the averaged shifts in the experiment are smaller than those in the theoretical calculation, and the tendency of the shifts is less consistent for each particle, such as much larger or smaller than the theoretical values. Despite this, our result provides the possibility to verify the ratio of the Leslie coefficients, α_2 and α_3, as well as changes by temperature with relatively fewer constraints because ϕ_c is found to be not dependent on rotation frequency or particle size.

B. Analysis of the region affected by flow

We observed textures around the rotating particle with controlling rotation frequency and particle size [Fig. 6(a)]. The region in which the director changes its alignment tends to widen with increasing rotation frequency and particle size. We compared the measured data to theoretical calculations that were performed by investigating the shifting tendency in Ericksen number by distance from the particle. While fixed characteristic quantities such as cell gap and particle size by system are used to describe the Ericksen number in general, we used an actual shear rate as characteristic quantities to consider properties of nonlinear changes in flow pattern (see Appendix A). The Ericksen number by position is

$$\mathrm{Er} = \frac{\eta(\nabla v)}{K/L^2}, \tag{9}$$

where η, v, K, and L are dynamics viscosity, velocity, elastic constant, and characteristic length, respectively. And we used 69 mPa s and 5 pN as η and K, respectively, and half the cell gap 30 μm as the characteristic length L [30]. We can consider that the director starts to deform by a viscous flow above the threshold value, called the critical Ericksen number (Er_c). Herein, Er_c is generally near 1 [35]. We can calculate the radius of the region in which the particle influences the director alignment by figuring out the critical distance corresponding to Er_c. An equation about a flow generated by a rotating particle not affected by external boundaries is well known; however, particles in our system are constrained in a cell with a gap comparable to particle size and affected by the proximity of the substrates. Because the system has low Re and the Navier-Stokes equation in that case becomes a form of the Laplace equation, we can find out the solution through the method of mirror images. The solution is as follows (see Appendix B):

$$\boldsymbol{v} = R^3\omega\rho\left\{\frac{C}{(\rho^2+z^2)^{\frac{3}{2}}} + \sum_{k=-\infty}^{\infty}\left[\frac{1}{(\rho^2+(z+2kd)^2)^{\frac{3}{2}}} - \frac{1}{(\rho^2+(z+2kd+2h)^2)^{\frac{3}{2}}}\right]\right\}\hat{\boldsymbol{\psi}}, \tag{10}$$

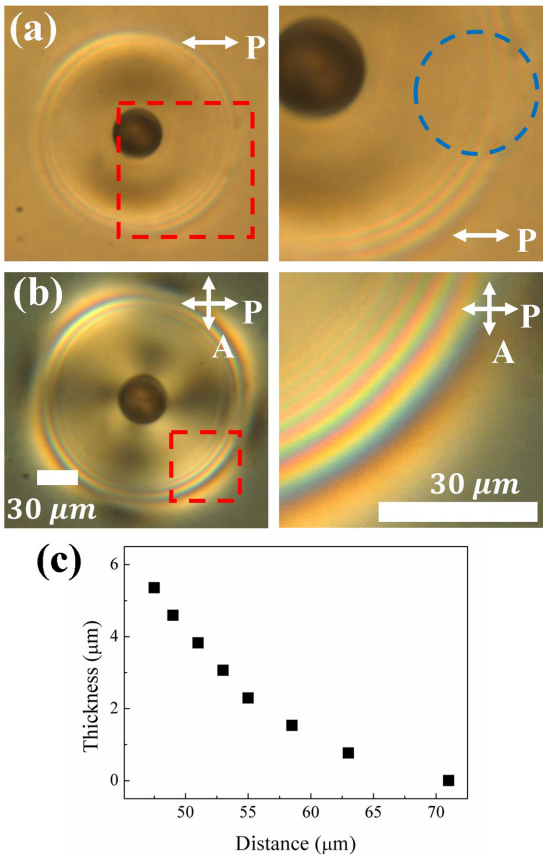

FIG. 7. (a) Images obtained through horizontally polarized light. An interference pattern is observed around the edge of the region affected by the flow. The particle rotates counterclockwise. In the right enlarged image, the interference pattern in the blue dashed circle is blurred because of a refractive index match. (b) Images obtained under crossed polarizers. The interference pattern in the images is easier to analyze than in (a) due to the clear contrast. (c) Graph of the thickness of the region where the director changes as a function of distance analyzed through the interference pattern.

where R, ω, ρ, z, and d are particle radius, rotation frequency, distance along the direction parallel to and perpendicular to the substrates from the center of the particle, and cell gap, respectively. $\hat{\boldsymbol{\psi}}$ is the unit vector along azimuthal direction. Furthermore, C is a coefficient of the correction term, which is empirically determined as 0.0259 to properly compensate the velocity at the surface. We put Eq. (10) into Eq. (9) and numerically calculated distances r_c that makes Er equal to Er_c with ω and R [Figs. 6(b) and 6(c)]. For an Er_c of 2.8, the calculation agrees with the experimental data.

C. Analysis of the interference pattern

We observed an interference pattern in the region affected by the flow [Figs. 7(a) and 7(b)]. This interference pattern appears under both configurations of one polarizer [Fig. 7(a)] and crossed polarizers [Fig. 7(b)], meaning that the phenomenon derives not by birefringence but by refractive index mismatch. In detail, a rotating particle forces the vertically aligned director to be parallel. Light experiences $n_{\mathrm{eff}}(\psi)$ in the region affected by the flow and n_o elsewhere, so that the light partially reflects on the boundaries between those two regions. The region affected by the flow is sandwiched between the regions not affected, so that light encounters two boundaries traveling along the z direction. This structure constructs the interferometer with varying thickness. The varying thickness produces an interference pattern. In general, in nematic colloidal systems, the director alignment around colloidal particles shows gradual changes over relatively long distances, so that the effective refractive index also changes gradually. In this case, a clear optical boundary does not appear, and thus it is difficult to observe a clear interference pattern. On the other hand, in our system, the director inside r_c at ψ has the same angle, while the director outside r_c is vertically aligned to the substrate. We can consider that the director abruptly changes over a relatively short distance in the vicinity of r_c. As a result, a clear optical boundary occurs with a distinct reflection. Furthermore, because the azimuthal angle of the director around a counterclockwise rotating particle at $\psi = -13^\circ$ is $\pi/2$, light with a horizontal linear polarization experiences n_o. Hence, the refractive index mismatch decreases near $\psi = -13^\circ$, and the optical boundary becomes ambiguous. The blue circle in Fig. 7(a) corresponds to the region near $\psi = -13^\circ$, where it can be seen that the interference pattern is blurred. This supports the explanation that the interference pattern is generated by a refractive index mismatch.

As previously mentioned, the velocity of the surface of a rotating particle is the largest at the equator and becomes smaller closer to the poles. Therefore, the distance between the particle and the edge of the region affected by the flow (i.e., the point where the director alignment is no longer influenced by the flow) in the xy plane becomes shorter closer to the poles. Therefore, the thickness of the region affected by the flow in the z direction decreases further away from the particle in the xy plane. We can estimate the thickness by considering that it varies following multiplication between the refractive index and integer multiples of the wavelength of visible light for repeated instances of the same color in the interference pattern [Fig. 7(c)]. We used the average refractive index of 5CB as 1.53 and the wavelength as 500 nm [40]. Although we conducted various trials to interpret this result theoretically, there were difficulties to obtain satisfying results. We leave this for future works with expectations that it is helpful to consider a role of height of particles and to calculate detailed viscous torque exerted on the director. In spite of the lack of theoretic approaches, we anticipate this approach helps to investigate visually a surrounding local flow of a rotating particle.

IV. CONCLUSIONS

We generated a local flow using microsized ferromagnetic spheres and a rotating magnetic field and then analyzed the NLC dynamics from the local flow. When Er is above a critical value, the director alignment changes. From the complete rotational symmetry of homeotropic alignment and rotation, the changed director alignment around a single particle also shows the same symmetry, and the stable angle in the region affected by the flow was determined only from the ratio between α_2 and α_3 regardless of any other variables except

temperature. The area of the region widened by increasing the rotation frequency, and we calculated this numerically through the Ericksen number and velocity profile. Furthermore, because the change of the director alignment generated by the local flow creates clear optical boundaries, an interference pattern was generated that is rarely observed. By analyzing the interference pattern, we estimated the thickness of the region in which the change of director alignment occurs. This indicates that we can visually analyze the motion of a flow around a particle in nematic fluids.

ACKNOWLEDGMENTS

This research was supported by the Basic Science Research Program through the National Research Foundation of Korea (NRF) funded by the Ministry of Education (NRF-2020R1A6A1A03047771, NRF-2021R1I1A3052203).

APPENDIX A: ERICKSEN NUMBER

The Ericksen number is a dimensionless quantity to depict hydrodynamics properties in simple manner [1,35,41,42]. This represents which effect between viscous flow and elasticity of a medium is dominant. The magnitude of the viscous flow is determined by viscosity and shear rate, and that of elasticity by elastic constants and the director change rate. Here, the former is expressed as $\eta\nabla v$ and the latter as $K\nabla^2 n$, where η, v, K, and n are dynamic viscosity, velocity, elastic constant, and the director, respectively. Simplifying the above two terms with representing the variables by characteristic quantities, we obtain

$$\mathrm{Er} = \frac{\eta V/L}{K/L^2} = \frac{\mu V L}{K}. \tag{A1}$$

This is a general form of Ericksen number, in which V and L are characteristic velocity and length. This could be proper if a shear rate is a constant or rarely changes like a flow between two parallel plates, one of which moves in tangential way to the other. On the other hand, we have to analyze a flow pattern with nonlinear shear rate in our system. Hence, fixed characteristic quantities like radius of the particle might not reflect actual properties of a flow around the particle. In this case, we consider that it is proper to use an actual shear rate of the flow around a rotating particle instead of characteristic shear rate *V/L*. From this, we obtain

$$\mathrm{Er} = \frac{\eta|\nabla v|}{K/L^2}. \tag{A2}$$

We use half the cell gap as characteristic length L. We can consider that the director around the particle starts to deform by viscous flow at higher Er than Er_c [25]. The critical Ericksen number is mainly near 1 and we empirically determined this in this paper.

APPENDIX B: A FLOW AROUND A ROTATING SPHERE SUSPENDED BETWEEN PARALLEL PLATES

Consider the Navier-Stokes equation for an incompressible flow,

$$\rho\frac{\partial \boldsymbol{v}}{\partial t} + \rho(\boldsymbol{v}\cdot\nabla)\boldsymbol{v} - \eta\nabla^2\boldsymbol{v} = -\nabla p + (\Delta\rho)g, \tag{B1}$$

where ρ is density of the flow, v velocity, η the dynamic viscosity, p pressure, and g gravitational acceleration. Because there is no flow in the background by pressure difference, we do not consider the effect of a density difference in our system and we consider that Δp and $\Delta\rho$ are zero:

$$\rho\frac{\partial \boldsymbol{v}}{\partial t} + \rho(\boldsymbol{v}\cdot\nabla)\boldsymbol{v} - \eta\nabla^2\boldsymbol{v} = \boldsymbol{0}. \tag{B2}$$

Substituting x_i/D, u/U, and tU/D by $x_i^{'}$, u', and t', Eq. (B2) becomes

$$\frac{\rho U^2}{D}\frac{\partial \boldsymbol{v}'}{\partial t'} + \frac{\rho U^2}{D}(\boldsymbol{v}'\cdot\nabla)\boldsymbol{v}' - \frac{\eta U}{D^2}\nabla^2\boldsymbol{v}' = \boldsymbol{0}, \tag{B3}$$

where D and U are characteristic length and velocity. Quantities that represent the system can be candidates of characteristic quantities: particle size, cell gap, and so on for characteristic length, and velocity of particle surface, relative velocity between two parallel plates, and so on for characteristic velocity.

Then, dividing Eq. (B3) with $\eta U/D^2$, we obtain

$$\frac{\rho UD}{\eta}\frac{\partial \boldsymbol{v}'}{\partial t'} + \frac{\rho UD}{\eta}(\boldsymbol{v}'\cdot\nabla)\boldsymbol{v}' - \nabla^2\boldsymbol{v}' = \boldsymbol{0}, \tag{B4}$$

where $\rho UD/\eta$ can be expressed as Reynolds number Re that is also a dimensionless quantity to help predict patterns of a flow by the ratio of inertial forces to viscous forces. Hence, we can neglect the first two terms of Eq. (B4) with the low Re that the effects of viscosity overwhelm those of inertia. Because NLCs have relatively high viscosity and the magnitude of flow around a particle is small, our system has low Re, and then Eq. (B4) becomes a form of the Laplace equation [43],

$$\nabla^2\boldsymbol{v} = \boldsymbol{0}. \tag{B5}$$

If the system follows the no-slip condition, the magnitude of flow has to be the same as the linear velocity of a rotating particle, the general solution satisfying the boundary condition of rotating particle sufficiently far from substrates is [44]

$$\boldsymbol{v} = \frac{R^3\omega}{r^2}\sin\eta\hat{\boldsymbol{\psi}}. \tag{B6}$$

In the above equation, R, ω, r, and η are radius of the particle, rotation frequency, distance from the center of the particle, and the polar angle, respectively. $\hat{\psi}$ means a unit vector of the direction of the azimuthal angle. Only the $\hat{\psi}$ direction of the velocity occurs due to the complete rotational symmetry. Here, we have to consider additional boundary conditions by two parallel substrates with the gap comparable to radius of the particle. We can satisfy the additional boundaries using the method of images [45].

Imagine that a rotating particle located at height h from the bottom substrate in the cell with gap d, which means the particle is d–h apart from the top substrate. Then, oppositely

rotating image particles to the real particle located at $-h$ and $2d-h$, respectively, make the magnitudes of flow at the bottom and top substrates zero; however, they hinder us from satisfying the boundary conditions at the opposite substrates. Hence, we need other image particles rotating with the same direction as the real particle and located at $-2d+h$ and $2d+h$. Nevertheless, the magnitudes of flow at both boundaries are slightly different from zero. This issue can be solved by locating infinite image particles at proper positions: particles of the same rotation direction as the real particle at $2kd+h$ and particles of the opposite direction at $2kd-h$, where k is an integer. Shifting the height of the coordinate system in $-h$ to adjust the center of the real particle as the origin, the particles with rotation direction of the same direction as and opposite direction to the real particle are located $2kd$ and $2kd-2h$, respectively; herein, a particle at $k=0$ is the real particle. Hence, we obtain

$$\boldsymbol{v} = R^3\omega\rho \sum_{k=-\infty}^{\infty}\left[\frac{1}{(\rho^2+(z+2kd)^2)^{\frac{3}{2}}} - \frac{1}{(\rho^2+(z+2kd+2h)^2)^{\frac{3}{2}}}\right]\hat{\boldsymbol{\psi}}, \tag{B7}$$

where z and ρ are distance along the direction perpendicular to and parallel to the substrates from the center of the particle and rotation direction of the real particle is assumed to be counterclockwise. The above image particles properly satisfy the boundary conditions at both substrates, whereas they break the boundary condition at the surface of the particle. We have to assume a new group of image particles regarding the real particle as a center to correct the boundary condition at the surface of the real particle, however, we just added a term enhancing effects of the real particle to simplify the equation:

$$\boldsymbol{v} = R^3\omega\rho\left\{\frac{C}{(\rho^2+z^2)^{\frac{3}{2}}} + \sum_{k=-\infty}^{\infty}\left[\frac{1}{(\rho^2+(z+2kd)^2)^{\frac{3}{2}}} - \frac{1}{(\rho^2+(z+2kd+2h)^2)^{\frac{3}{2}}}\right]\right\}\hat{\boldsymbol{\psi}}, \tag{B8}$$

where C is a quite small as 0.0259 and was empirically determined to well correct the boundary condition. With the small correction term, the Eq. (B8) explains finely flow patterns by h around a rotating particle except when the particle is highly close to either substrate. As an absolute value of k increases, the value of each term in Eq. (B8) drastically decreases, so that v saturates at a small $|k|$. We numerically analyzed our experimental results using the Eq. (B8), and we set a range of k from -10 to 10.

[1] P. G. de Gennes and J. Prost, *The Physics of Liquid Crystals*, 2nd ed. (Oxford University Press, Oxford, 1993).
[2] P. J. Collings and M. Hird, *Introduction to Liquid Crystals* (Taylor & Francis, London, 1997).
[3] A. Rapini and M. Papular, J. Phys. Colloq. **30**, C4 (1969).
[4] W. W. Beens and W. H. de Jeu, J. Chem. Phys. **82**, 3841 (1985).
[5] J. Whal and F. Fischer, Mol. Cryst. Liq. Cryst. **22**, 359 (1973).
[6] J. A. Müller, R. S. Stein, and H. H. Winter, Rheol. Acta **33**, 473 (1994).
[7] D. M. Boudreau, H. H. Winter, C. P. Lillya, and R. S. Stein, Rheol. Acta **38**, 503 (1999).
[8] I. Jánossy, P. Pieranski, and E. Guyon, J. Phys. (Paris) **37**, 1105 (1976).
[9] T. Börzsönyi, Á. Buka, A. P. Krekhov, and L. Kramer, Phys. Rev. E **58**, 7419 (1998).
[10] E. Guazzelli and E. Guyon, J. Phys. (Paris) **43**, 985 (1982).
[11] P. Pieranski and E. Guyon, Phys. Rev. Lett **39**, 1280 (1977).
[12] T. Börzsönyi, Á. Buka, A. P. Krekhov, O. A. Scaldin, and L. Kramer, Phys. Rev. Lett **84**, 1934 (2000).
[13] A. P. Krekhov and L. Kramer, Phys. Rev. E **72**, 031705 (2005).
[14] A. D. Rey and M. M. Denn, J. Non-Newton. Fluid Mech. **27**, 375 (1988).
[15] F. M. Leslie, J. Fluid Mech. **18**, 595 (1964).
[16] M. Miesowicz, Nature (London) **158**, 27 (1946).
[17] F. M. Leslie, Q. J. Mech. Appl. Math. **19**, 357 (1966).
[18] J. L. Ericksen, Mol. Cryst. Liq. Cryst. **7**, 153 (1969).
[19] F. M. Leslie, Arch. Ration. Mech. Anal. **28**, 265 (1968).
[20] F. M. Leslie, *Advances in Liquid Crystals* (Elsevier, Amsterdam, 1979).
[21] G. Toth, C. Denniston, and J. M. Yeomans, Phys. Rev. Lett. **88**, 105504 (2002).
[22] D. Svensek and S. Zumer, Phys. Rev. E **66**, 021712 (2002).
[23] F. Brochard, Mol. Cryst. Liq. Cryst. **23**, 51 (1973).
[24] D. Svensek and S. Zumer, Liq. Cryst. **28**, 1389 (2001).
[25] P. Pieranski and E. Guyon, Solid State Commun. **13**, 435 (1973).
[26] P. Pieranski and E. Guyon, Phys. Rev. A **9**, 2814 (1974).
[27] P. Pieranski and E. Guyon, Phys. Lett. A **49**, 237 (1974).
[28] C. Gähwiller, Mol. Cryst. Liq. Cryst. **20**, 301 (1973).
[29] G. P. Chen, H. Takezoe, and A. Fukuda, Liq. Cryst. **5**, 341 (1989).
[30] A. G. Chmielewski, Mol. Cryst. Liq. Cryst. **132**, 339 (1986).
[31] H. Wang, T. X. Wu, S. Gauze, J. R. Wu, and S.-T. Wu, Liq. Cryst. **33**, 91 (2006).
[32] C. Wu, T. Qian, and P. Zhan, Liq. Cryst. **34**, 1175 (2007).
[33] J. B. Rovner, D. S. Borgnia, D. H. Reich, and R. L. Leheny, Phys. Rev. E **86**, 041702 (2012).
[34] B. A. van Tiggelen, R. Maynard, and A. Heiderich, Phys. Rev. Lett. **77**, 639 (1996).
[35] P. Oswald and P. Pieranski, *Nematic and Cholesteric Liquid Crystals: Concepts and Physical Properties Illustrated by Experiments* (CRC press, Boca Raton, FL, 2005).
[36] M. Cui and J. R. Kelly, Mol. Cryst. Liq. Cryst. **331**, 49 (1999).
[37] K. Skarp, S. T. Lagerwall, and B. Stebler, Mol. Cryst. Liq. Cryst. **60**, 215 (1980).
[38] H. Herba, A. Szymanski, and A. Drzymala, Mol. Cryst. Liq. Cryst. **127**, 153 (1985).

[39] H. Kneppe, F. Schneider, and N. K. Sharma, J. Chem. Phys. **77**, 3203 (1982).
[40] J. Li, C. H. Wen, S. Gauze, R. Lu, and S. T. Wu, J. Disp. Technol. **1**, 51 (2005).
[41] J. L. Ericksen, Trans. Soc. Rheol. **13**, 9 (1969).
[42] J. L. Ericksen, Trans. Soc. Rheol. **4**, 29 (1960).
[43] H. Hapel and B. H. Brenner, *Low Reynolds Number Hydrodynamics: With Special Applications to Particulate Media* (Springer Science & Business Media, New York, 2012).
[44] R. L. Fosdick and B. G. Kao, Rheol. Acta. **19**, 675 (1980).
[45] G. B. Jeffery, Proc. Lond. Math. Soc. **2**, 327 (1915).